REVIEW

National Science Open
5: 20260029, 2026
https://doi.org/10.1360/nso/20260029

Materials Science

Special Topic: Hollow Multishelled Structure

Interfacial engineering of hollow multishelled structure for metal-air batteries: Reaction mechanism and material design

Penghui Shang[1,2], Di Li[1,2], Dewen Hou[1,2], Jiangyan Wang[1,2], Jiawei Wan[1,2,*], Ranbo Yu[3,*] & Dan Wang[1,2,3,*]

[1]*State Key Laboratory of Biopharmaceutical Preparation and Delivery, Institute of Process Engineering, Chinese Academy of Sciences, Beijing 100190, China;*
[2]*University of Chinese Academy of Sciences, Beijing 100049, China;*
[3]*College of Chemistry and Environment Engineering, Shenzhen University, Shenzhen 518060, China*

*Corresponding authors (emails: jwwan@ipe.ac.cn (Jiawei Wan); ranboyu@szu.edu.cn (Ranbo Yu); danwang@szu.edu.cn (Dan Wang))

Received 2 March 2026; Revised 9 April 2026; Accepted 15 April 2026; Published online 16 April 2026

Abstract: Metal-air batteries (MABs) possess high theoretical energy density, but their practical applications are often restricted by unstable multiphase interfaces as well as mismatched mass transport and reaction kinetics. This review first outlines the operating principles of non-aqueous, aqueous, and solid-state MABs, highlights their key differences, and then summarizes the evolution characteristics of major interfaces during cycling, including the metal anode/electrolyte interface, the air cathode/electrolyte interface, and separator/electrolyte contact interfaces. The typical problems encountered in MABs include pore blockage caused by product accumulation, which reduces the effective reaction area of the cathode; increased resistance resulting from electrolyte decomposition and side reactions; anode corrosion or passivation accompanied by non-uniform deposition; and contact degradation induced by volume change and internal stress. We discuss the hollow multishelled structure (HoMS) as a potential platform, which can play roles in product buffering, transport pathway maintenance, and structural cushioning. Finally, we emphasize the importance of quantitative validation, coordinated interface design, and performance evaluation under practical working conditions, with the support of data analysis and AI tools.

Keywords: metal-air batteries, hollow multishelled structure, interface engineering, stabilization, mass transport

INTRODUCTION

Driven by the global "dual-carbon" targets and the ongoing energy transition, the rapid growth in demand for renewable electricity has imposed more stringent requirements on energy storage technologies in terms of energy density, cycle life, safety, and cost. These requirements are particularly crucial for effectively mitigating the intermittency of wind and solar power generation [1–3]. Meanwhile, the accelerated electrification of transportation and the sustained growth in demand for industrial and portable applications further highlight the inherent limitations of conventional lead-acid batteries, nickel-metal hydride batteries, and even lithium-ion batteries in terms of energy density, service life, environmental impact, and resource supply [4–6]. Therefore, developing high-performance and environmentally benign energy storage technologies is an

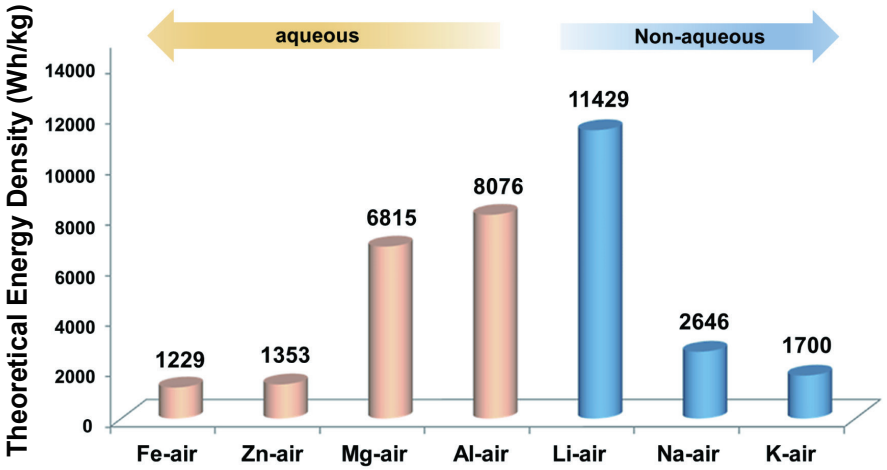

Figure 1 Theoretical energy densities for different types of metal-air batteries. Reproduced with permission from Ref. [11]. Copyright©2017, American Chemical Society.

important pathway toward carbon-neutral energy systems [7]. Among various candidate technologies, metal-air batteries (MABs) have attracted extensive attention due to their ultrahigh theoretical energy density, abundant raw materials, and potential environmental compatibility [8–10]. To highlight the intrinsic potential of MABs, Figure 1 summarizes the theoretical energy densities of various metal-air systems. Among them, Li-air and Al-air batteries exhibit exceptionally high theoretical gravimetric energy densities, which are far higher than those of conventional battery technologies [11]. However, their practical development is severely restricted by the instability of multiphase interfaces [12–14]. The structure and stability of the metal anode interface and air cathode interface directly govern charge transfer, ion transport, and reaction kinetics inside the battery cell [15–17]. Accordingly, deliberate design and precise construction of interfacial architectures in MABs can improve energy efficiency and cycling stability under practical operation conditions, while enhancing rate capability and operational reliability [18–21].

Interfacial modification engineering is a key approach to improving battery performance. It reconstructs the composition and structure of interfaces through physical, chemical, or materials-engineering methods, thereby optimizing the coupling between charge transfer and ion transport [22–25], regulating the adsorption-desorption kinetics of reaction intermediates at interfaces [26–28], and suppressing interfacial failure events to achieve synergistic enhancement of battery performance [29,30]. MABs commonly suffer from multiphase interfacial instabilities, including dendrite growth, passivation and corrosion, side reactions, and transport blockage, as well as interfacial delamination induced by product accumulation. These issues lead to increased polarization and shortened cycle life. A variety of modification strategies have been reported to address these interfacial challenges. For example, at the cathode interface, surface iron vacancies in a garnet-structured $Fe_2Mo_3O_{12}$ catalyst have been shown to promote O_2 activation while maintaining structural stability [31]. At the anode interface, an Mg-0.1Ca alloy can simultaneously refine grains and regulate the passivation layer, thereby suppressing self-corrosion while preserving ion transport [32]. In solid-state systems, an integrated interface enabled by a lithium-exchanged X-type zeolite membrane (LiXZM) can reduce contact resistance and block H_2O/CO_2, thus mitigating parasitic reactions [8]. In addition, crystal-structure regulation, doping and hybridization, single-atom site engineering, electrolyte additives, and metal

alloying have all been demonstrated to significantly improve battery performance [33–37]. Nevertheless, precise mechanistic control, multi-interface compatibility, and scalable long-term stability remain key challenges [38–40].

In recent years, hollow multishelled structure (HoMS) materials have developed rapidly in the field of energy conversion and storage [41,42]. As a novel hierarchical architecture, HoMS integrates multi-chamber void spaces with thin, permeable shells. Electrodes based on HoMS can substantially expand the electrochemically active surface area, create shorter electron/ion transport pathways, and provide effective volume-strain buffering. These advantages facilitate the confined transport and efficient conversion of reactants/intermediates in various battery systems (e.g., lithium-sulfur batteries and metal-anode chemistries) and enable more uniform regulation of ionic flux [41,43–45]. Based on these structural advantages, HoMS-enabled interfacial engineering is expected to bring benefits to MABs. On the cathode side, HoMS may alleviate pore blockage and collapse of triple-phase boundaries caused by the accumulation of discharge products, thereby reducing local mass-transfer limitations and polarization during the oxygen reduction reaction (ORR) and oxygen evolution reaction (OER) [46]. On the anode side, HoMS may improve deposition uniformity and suppress corrosion, dendrite growth, and passivation, thus enhancing cycling stability and safety [47].

Accordingly, this review first introduces the working principles of different metal-air batteries and the distinctions among their system configurations. It then systematically discusses the composition of the key interface and the associated issues, including the metal anode interface and the air cathode interface. Typical failure mechanisms are summarized, such as product blockage and pore deactivation, side reactions and electrolyte decomposition, anode corrosion/passivation and dendrite growth, and interfacial delamination and contact instability. Next, applications of HoMS materials for addressing similar issues in other battery systems are introduced, with particular emphasis on how HoMS, as a hierarchical architecture, can resolve key interfacial bottlenecks in MABs through product/intermediate management, interface stabilization, transport-pathway construction, and mechanical buffering. Finally, perspectives are provided on practical implementation routes for multi-interface co-design under realistic operating conditions, quantitative mechanistic validation, and scalable construction, together with opportunities and research directions for the predictive interface design of HoMS-based systems.

REACTION MECHANISM OF METAL-AIR BATTERIES

The fundamental working of metal-air batteries relies on the electrochemical coupling between metal oxidation/reduction at the anode and oxygen reduction/evolution (ORR/OER) at the air cathode (Figure 2) [10]. The electrolyte (non-aqueous, aqueous, or solid-state) dictates reaction pathways, discharge products, and interfacial characteristics, leading to system-dependent mechanisms and bottlenecks [48,49].

Non-aqueous metal-air batteries

As shown in Figure 3 [50], lithium-air batteries can be classified into aprotic (Figure 3a), aqueous (Figure 3b), solid-state (Figure 3c), and mixed aqueous/aprotic systems (Figure 3d) according to electrolyte

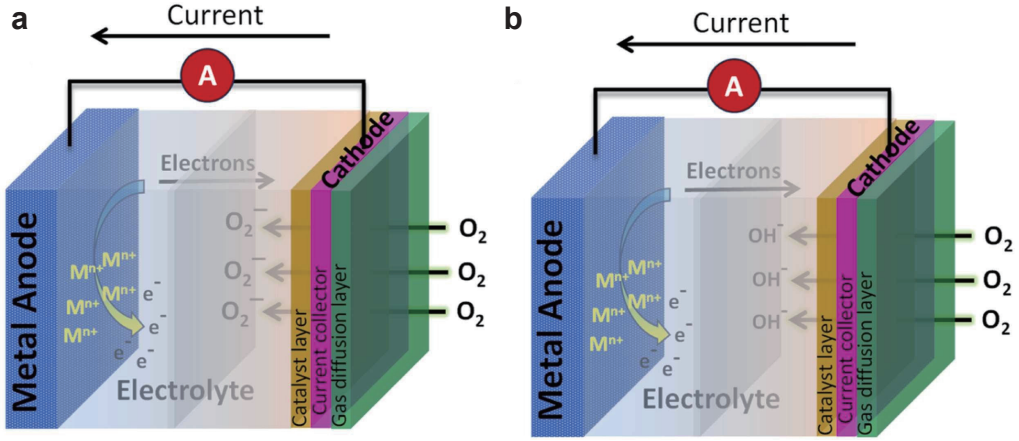

Figure 2 Schematic representations of the primary chemical reactions occurring in metal-air batteries with (a) non-aqueous and (b) aqueous electrolytes. Reproduced with permission from Ref. [10]. Copyright©2025, Elsevier.

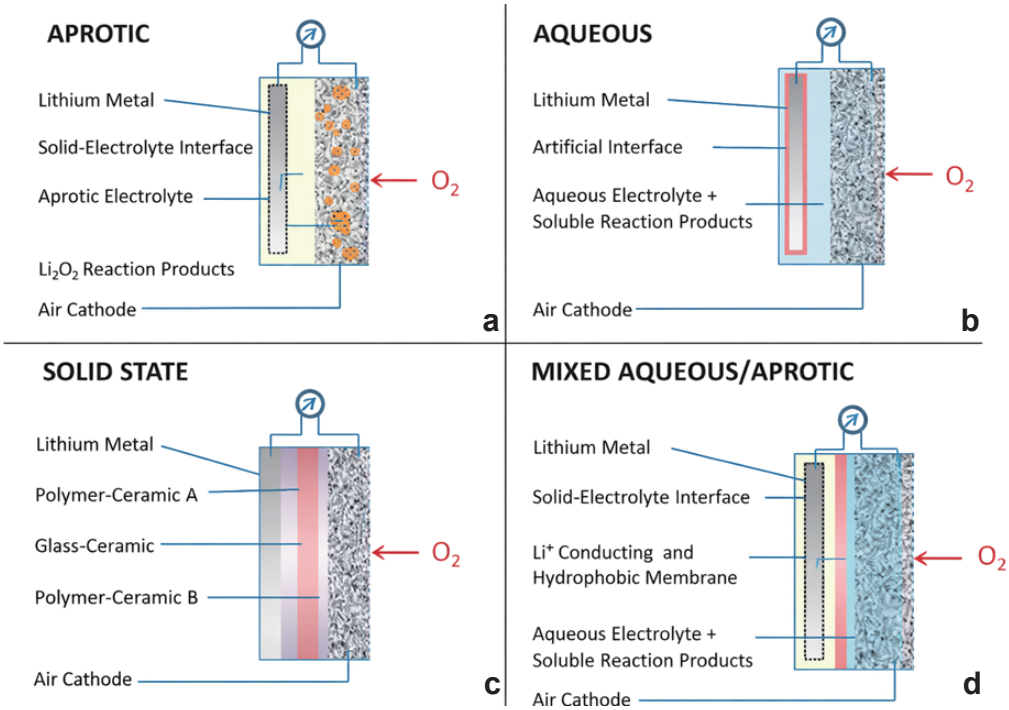

Figure 3 Four different structural lithium-air batteries. (a) Aprotic liquid electrolyte; (b) aqueous-based liquid electrolyte; (c) all-solid-state liquid electrolyte; (d) aprotic-aqueous mixed-type liquid electrolyte. Reproduced with permission from Ref. [50]. Copyright©2010, American Chemical Society.

configuration, and each system exhibits distinct interfacial characteristics. Aprotic systems use organic electrolytes to avoid the direct reaction between highly reactive alkali metals (e.g., Li, Na) and water, but they are often limited by electrolyte decomposition, parasitic reactions, and cathode passivation. Aqueous systems offer higher ionic conductivity, yet they suffer from corrosion and parasitic reactions. Solid-state systems improve safety by eliminating liquid electrolytes, but are generally restricted by poor solid-solid interfacial contact, high interfacial resistance, and insufficient interfacial stability during cycling. Mixed systems

integrate non-aqueous and aqueous components to balance anode stability and cathode reaction kinetics, but they also introduce additional challenges, including interfacial incompatibility, ion-transfer resistance, and electrolyte crossover. Regardless of the system type, the electrolyte must satisfy several key requirements, including high ionic conductivity, sufficient electrochemical stability, good electrode compatibility, and long-term cycling durability [51,52].

The electrode reactions in non-aqueous metal-air batteries involve the coupled processes of metal oxidation and oxygen reduction. Taking non-aqueous Li-air batteries (LABs) as a representative example, the main reaction pathway can be described as follows [8].

Reaction at the anode: $Li \rightarrow Li^+ + e^-$

Reaction at the cathode: $2Li^+ + O_2 + 2e^- \rightarrow Li_2O_2$

Overall reaction: $2Li + O_2 \rightarrow Li_2O_2$

The working mechanism of Li-air batteries is based on the coupling of lithium oxidation/reduction at the anode and oxygen reduction/evolution reactions at the air cathode, with discharge products (typically Li_2O_2 in aprotic systems) forming and decomposing during cycling [50]. The electrolyte and catalysts play important roles in determining the type and crystal structure of discharge products. Although Li-air batteries possess outstanding theoretical energy density, their practical performance is still largely limited by interfacial challenges [9].

(1) Electrolyte decomposition and parasitic reactions. Organic electrolytes usually undergo oxidative decomposition at high potentials around 4.0 V and may also react with reactive ORR/OER intermediates such as O_2^- and LiO_2, leading to the formation of insulating byproducts including Li_2CO_3, LiOH, and lithium formate (HCO_2Li) [53]. Freunberger *et al*. [54] showed that carbonate-based electrolytes react with LiO_2 to form Li_2CO_3 and CO_2. Moreover, the high decomposition barrier of Li_2CO_3 during OER further contributes to cathode clogging and rapid capacity decay.

(2) Cathode passivation and limited reversibility. The morphology and deposition mode of solid Li_2O_2 critically affect the performance of Li-air batteries. In particular, large particle sizes and high crystallinity hinder the transport of oxygen and electrolyte, thereby promoting cathode passivation [55].

Aqueous metal-air batteries

Non-aqueous metal-air batteries can generally deliver higher theoretical energy densities and distinct discharge chemistries, such as the formation of Li_2O_2. However, they still face major challenges, including electrolyte and interfacial instability, carbonate by-product formation, large reaction overpotentials, and concerns related to safety and cost. In contrast, aqueous electrolytes in metal-air batteries (such as alkaline electrolytes of KOH/NaOH [56] and acidic electrolyte of H_2SO_4 [57]) have a higher ionic conductivity, lower cost, and better safety. Their discharge products are often deposited in the form of hydroxides or oxides, making these systems more compatible with practical engineering applications. Nevertheless, aqueous systems also suffer from evident drawbacks, including water decomposition and corrosion-related side reactions such as hydrogen evolution and metal self-corrosion/passivation. In addition, although aqueous systems generally provide higher ionic conductivity, the kinetics of ORR and OER can still be sluggish and strongly influenced by electrolyte chemistry, catalyst properties, and interfacial mass transport [57].

In aqueous MABs, the fundamental mechanism follows metal oxidation at the anode coupled with oxygen

reduction at the cathode. ORR commonly proceeds as follows: In neutral and alkaline electrolytes, $O_2 + 2H_2O + 4e^- \rightarrow 4OH^-$; while in acidic media, $O_2 + 4H^+ + 4e^- \rightarrow 2H_2O$. Alkaline media generally offer faster ORR kinetics and more stable discharge voltages [58].

The air cathode-electrolyte interface is the region where the ORR occurs during discharge, and the OER proceeds during charge. The effective reaction zone is generally at the region where oxygen, the solid electrode framework, and the electrolyte are simultaneously connected [59,60]. In liquid-electrolyte systems, this zone is established by gaseous O_2, the solid catalyst layer with a conductive framework, and the liquid electrolyte. Its area and connectivity determine whether oxygen supply matches ion supply [61]. In solid-state systems, the reaction zone becomes a cooperative contact region among gaseous O_2, the solid air electrode, and the solid electrolyte. This region is usually smaller and depends more strongly on interfacial contact quality and microstructure design [62]. The governing mechanism at the air cathode can be understood as the coupling of reaction kinetics and multicomponent mass transport. On the one hand, the electronic structure of active sites, together with charge redistribution and band alignment at the catalyst-support interface, determines the binding of reaction intermediates and the reaction pathway, thereby influencing the energy barriers and reaction selectivity [60]. On the other hand, oxygen diffusion, electrolyte wetting, pore tortuosity, and ion migration jointly determine local concentration gradients and potential distribution [63]. In addition, the microstructure at the catalyst-conductive framework interface determines whether active sites can be fully utilized and remain stable under high current densities. Therefore, the air cathode requires the coordination of intrinsic site activity, charge-transfer efficiency, and mass-transport efficiency. Catalysts are commonly loaded onto conductive frameworks in the form of nanoparticles, defect-rich structures, single-atom sites, or heterojunctions, and together with binders and pore structures, they form a connected reaction network [63]. This network must provide fast electron transport and strong interfacial adhesion, while maintaining continuous ion and gas transport pathways to stabilize the reaction zone. During cycling, the nucleation and growth of discharge products or precipitates continuously reshape the pore structure and wetting behavior, thereby altering the spatial distribution of the reaction zone [64]. As products gradually accumulate and fill the pores, the connected pathways for oxygen diffusion and electrolyte infiltration decrease. As a result, the effective reaction zone shrinks, transport polarization becomes more pronounced, and the overpotential rises rapidly [65]. The specific manifestation depends on the electrolyte system. In non-aqueous cells, discharge products and electrolyte decomposition products often co-deposit on the cathode surface and inside pores, blocking active sites, increasing interfacial resistance, and making product decomposition during charge more difficult. These effects further accelerate electrolyte decomposition and form a self-aggravating cycle [66]. In aqueous cells, solid precipitates and gas bubbles occupy the pores and disrupt the continuous wetting of the catalyst layer, thereby blocking oxygen and ion transport, shifting the controlling factor from reaction kinetics toward mass transport, and causing voltage fluctuation and reduced energy efficiency [14]. In solid-state cells, if the contact among gaseous O_2, the air electrode, and the solid electrolyte develops microcracks or gaps owing to stress or volume changes, the effective reaction zone becomes weakened and discontinuous. As a result, contact resistance increases and is difficult to recover in the absence of a re-wetting process, ultimately leading to capacity loss and poor rate performance [67]. Meanwhile, if the bonding at the catalyst-support interface is weak or the conductive network is discontinuous, active sites cannot be effectively utilized and may detach or deactivate under cycling stress, bubble impact, or volume changes. Under high OER potentials, corrosion of carbon supports further weakens

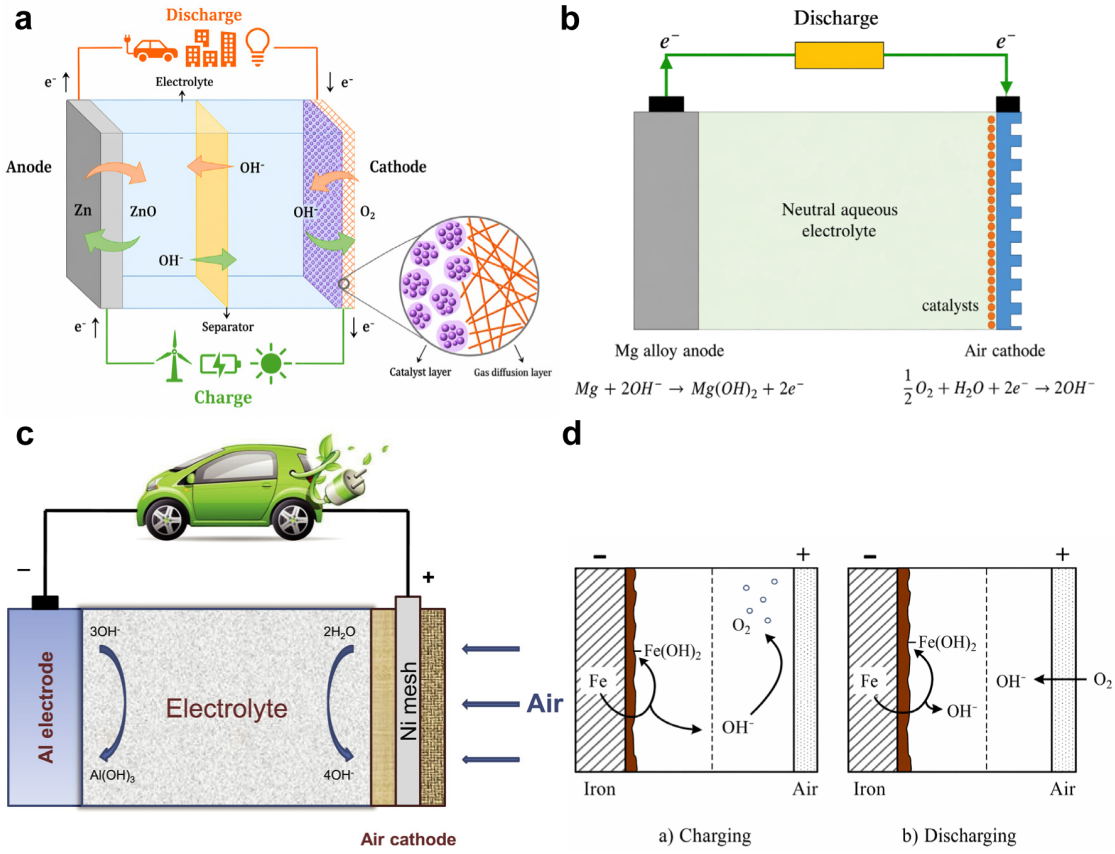

Figure 4 The working principles of four types of metal-air batteries. (a) Zn-air battery. Reproduced with permission from Ref. [70]. Copyright©2022, Elsevier. (b) Mg-air battery. Reproduced with permission from Ref. [71]. Copyright©2021, Elsevier. (c) Al-air battery. Reproduced with permission from Ref. [72]. Copyright©2021, Elsevier. (d) Fe-air battery. Reproduced with permission from Ref. [3]. Copyright©2014, John Wiley and Sons.

the conductive framework and induces pore collapse, which in turn aggravates interfacial deterioration [68]. In addition, dissolution, aggregation, or phase transformation of metal components reduces the number of accessible active sites and alters the local electronic structure, thereby slowing the reaction kinetics [69]. Therefore, the design of the air cathode interface and catalyst-layer design should simultaneously consider intrinsic catalytic activity, efficient electron/ion transport, and long-term structural stability, so as to mitigate irreversible performance loss caused by microstructural degradation and product blockage.

The discharge products formed on the metal anode are typically metal oxides or hydroxides, which generally exhibit good environmental compatibility. For example, Zn-air yields ZnO (Figure 4a) [70], Mg-air yields $Mg(OH)_2$ (Figure 4b) [71], Al-air involves soluble AlO_2^- and minor $Al(OH)_3$ (Figure 4c) [72], and Fe-air batteries generally involve the formation of iron hydroxides/oxyhydroxides and related iron oxide species, depending on electrolyte composition and operating conditions (Figure 4d) [3]. The morphology and compactness of these products strongly influence interfacial transport.

The metal anode-electrolyte interface is the starting region for metal dissolution/deposition or redox reactions, and it also serves as the key pathway for ions to enter the electrolyte and complete the current loop [73]. In non-aqueous systems, highly reactive metals rapidly form a solid electrolyte interphase (SEI) upon contact with organic electrolytes. This SEI usually consists of mixed inorganic and organic components [53].

An ideal interphase should block electron transport, maintain high ionic conductivity for metal ions, and remain continuous under fluctuations in current density and volume changes [74]. In aqueous systems, the interface is more prone to hydrogen evolution and self-corrosion, while reaction products are often deposited as oxides or hydroxides to form a dynamic passivation layer [70]. In solid-state systems, the anode and solid electrolyte form a solid-solid contact, where interfacial defects, voids, and space-charge effects can significantly increase contact resistance [52]. Any growth of a reaction layer or loss of contact area can directly intensify polarization. These compositions and processes determine the uniformity and reversibility of anode reactions.

Typical failures of metal anodes do not result from a single process, but rather from the coupled evolution of non-uniform deposition, corrosion, passivation, gas evolution, and dead-metal formation. In many systems, local surface defects, micro-protrusions, and heterogeneous ion-flux initially induce uneven deposition/dissolution and surface roughening, which can further evolve into dendrite growth through the intensified tip effect [29,38]. Once formed, dendrites not only increase the risk of internal short circuits and safety hazards, but also promote the generation of electrically isolated dead metal and reduce coulombic efficiency [70]. Meanwhile, side reactions continuously reshape the anode-electrolyte interface. In aqueous environments, self-corrosion and hydrogen evolution consume active metal, alter local interfacial chemistry, and disturb the effective reaction area through bubble accumulation, thereby further aggravating deposition heterogeneity [75]. For metals that are prone to passivation, such as Fe in iron-air batteries, the continuous formation and densification of oxide/hydroxide films hinder ion transport, increase interfacial resistance, and gradually convert local interfacial instability into persistent electrochemical inactivity [76]. As illustrated in Figure 5a–c, dendrite formation, self-corrosion, hydrogen evolution, and passivation-layer growth on Zn are strongly interconnected and collectively lead to dead Zn formation and accelerated loss of active material [75,77,78]. Similarly, Figure 5d shows that self-corrosion of Mg produces insoluble $Mg(OH)_2$, while impurities, defects, and intermetallic compounds can further accelerate corrosion and hydrogen evolution; the resulting passivation film hinders Mg^{2+} transport and leads to increased polarization and capacity fading [71]. Therefore, the degradation of metal anodes can be understood as a coupled failure-evolution process, in which interfacial side reactions, transport deterioration, and structural instability mutually reinforce each other. Accordingly, the key objectives of anode interfacial regulation are to homogenize ion flux, suppress corrosion and parasitic reactions, control passivation-layer evolution, and buffer volume and stress changes, so as to prevent a reversible interface from evolving into irreversible degradation.

Besides the metal anode-electrolyte and air cathode-electrolyte interfaces, some metal-air batteries also contain a separator between the two electrodes [79]. The role of the separator is not limited to physically isolating the electrodes and preventing short circuits. It also affects ion-selective transport, suppresses undesired species crossover, and influences the uniformity of current distribution inside the cell [80]. In liquid-electrolyte systems, the electrolyte fills the pores of the separator and provides pathways for ion transport. However, these pores may also allow dissolved species to migrate to the counter electrode. In addition, precipitates or decomposition products can accumulate inside the pores, and such blockage and contamination further increase internal resistance [79]. If solid products preferentially deposit on one side of the separator, ions will tend to concentrate in a few relatively open regions, resulting in local current concentration. This makes anode reactions more non-uniform and raises the risk of dendrite growth. In solid-state systems, efficient ion conduction requires intimate contact between the solid electrolyte and both

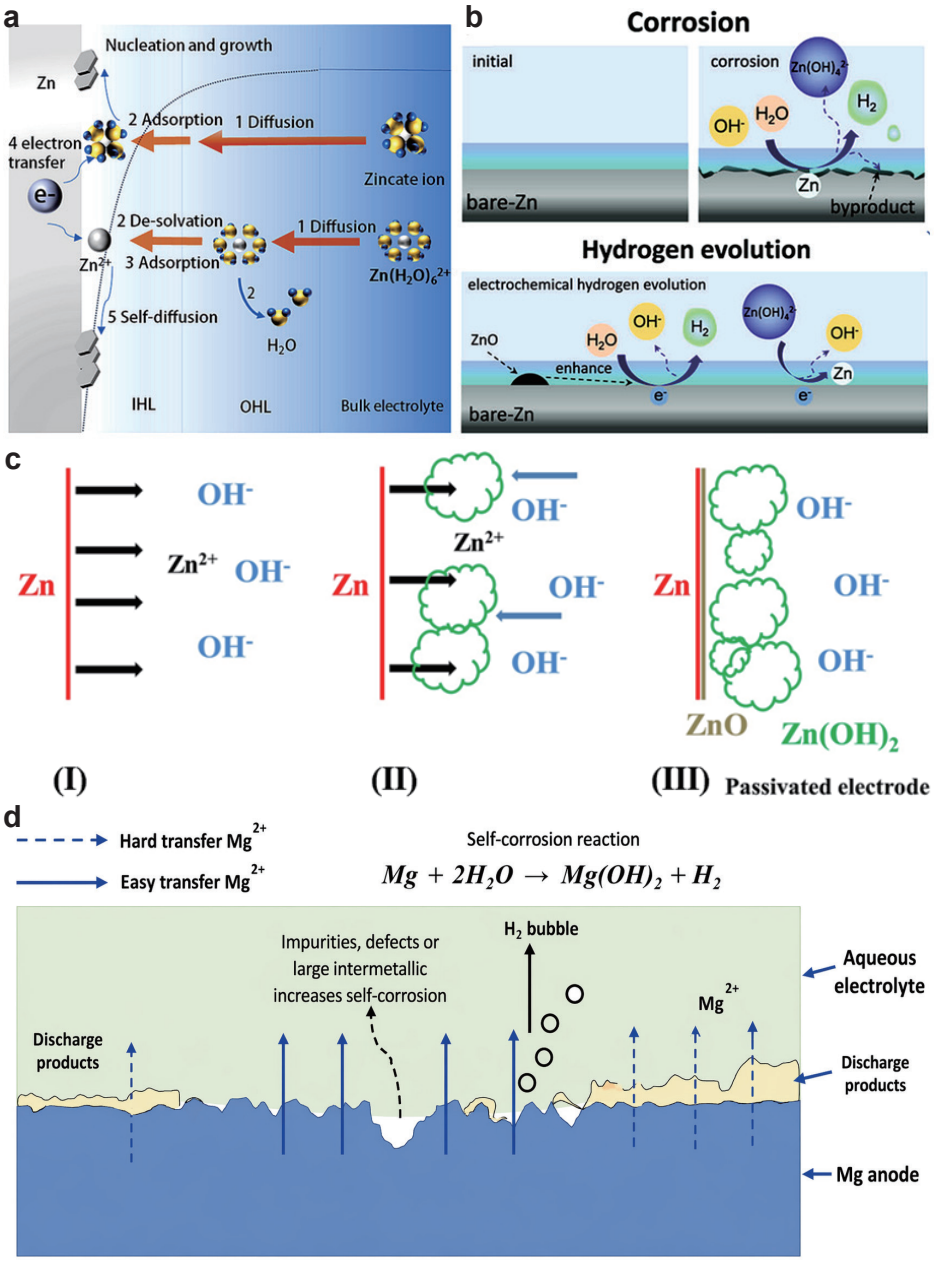

Figure 5 (a) Process of zinc deposition. Reproduced with permission from Ref. [77]. Copyright©2022, Royal Society of Chemistry. (b) The self-corrosion and hydrogen evolution of the zinc metal anode. Reproduced with permission from Ref. [75]. Copyright©2023, John Wiley and Sons. (c) The formation process of the zinc anode passivation layer. Reproduced with permission from Ref. [78]. Copyright©2016, John Wiley and Sons. (d) Reactions on the surface of the magnesium anode. Reproduced with permission from Ref. [71]. Copyright©2021, Elsevier.

electrodes. During cycling, the thickening of reaction layers, the loss of interfacial contact, or the increase in internal blockage can gradually increase interfacial resistance and intensify polarization [52]. Meanwhile, side reactions and electrolyte decomposition may generate persistent deposits at different locations and alter the local interfacial environment, leading to a continuous increase in resistance and a gradual decline in electrochemical activity [81]. Therefore, separator and electrolyte interfacial optimization should keep ion

pathways continuously open, reduce deposit accumulation and species crosstalk, and maintain sufficient mechanical strength and conformal contact to avoid penetration or cracking. These factors are essential for achieving long-term stable operation.

Therefore, during operation, metal-air batteries involve the metal anode interface, the air cathode interface, and the separator/electrolyte contact interface. These interfaces govern the coupled transport of electrons and ions, the diffusion and supply of oxygen and reactants, and the adsorption and conversion of intermediates at active sites. More importantly, these interfaces are not static boundaries. During repeated discharge/charge, their chemical composition and microstructure continuously evolve. Once local mass transport becomes restricted, polarization and concentration gradients accumulate, or volume change and stress are further intensified, the system may gradually shift from reversible cycling to irreversible degradation and failure. Therefore, effective structural and chemical regulation of these key interfaces is one of the main strategies for improving the efficiency and lifetime of metal-air batteries.

ADVANTAGES OF HOMS FOR ENERGY STORAGE BATTERIES

HoMSs are representative hierarchical hollow materials composed of multiple concentric shells separated by internal voids [82]. Their tunable shell-cavity units provide a large accessible surface area and abundant interfaces, shorten the diffusion paths of ions and electrons, and relieve product accumulation and stress buildup through multilevel confinement and structural buffering. HoMS can be synthesized through hard-templating routes, such as layer-by-layer coating followed by template removal by etching, soft-templating routes using micelles or vesicles to direct multilayer interfacial growth, or template-free routes based on self-assembly, Ostwald ripening, and the Kirkendall effect to construct multishelled hollow architectures [82]. In 2009, Wang and co-workers [83] proposed the sequential templating approach (STA) (Figure 6a), which provides a general strategy for controllable synthesis of HoMS. In STA, a sacrificial template serves as the starting point, while precursors continuously accumulate on the template surface to form shells. Repeated templating and deposition then drive shell growth from the inside outward, ultimately producing concentric multishell and multicavity structures. Since then, an increasing number of studies on HoMS based on STA have been reported (Figure 6b) [84]. In terms of structural design, HoMS exhibits high flexibility (Figure 6c) [83]. Their particle size and composition, shell thickness and pore structure, shell number and spacing, as well as subsequent surface or pore modifications, can all be adjusted. By combining these factors, HoMS can better meet the needs of different applications in terms of mass transport, stability, and active-site accessibility. To date, HoMS have attracted broad interest in energy storage and electrocatalysis, sensing, and drug delivery [81,85–89]. In particular, the combined features of confinement, cross-shell transport, and chemical/mechanical buffering make HoMS promising for mitigating multiphase interfacial bottlenecks in MABs.

HoMS provides multi-level void space to accommodate volume changes

For HoMS-based interfacial layers on metal anodes, the primary goal is to achieve uniform ion flux and stable interfacial contact, thereby mitigating dendrite growth and interphase instability. This requirement reflects the inherently coupled nature of metal-anode failure, which involves the interplay of non-uniform

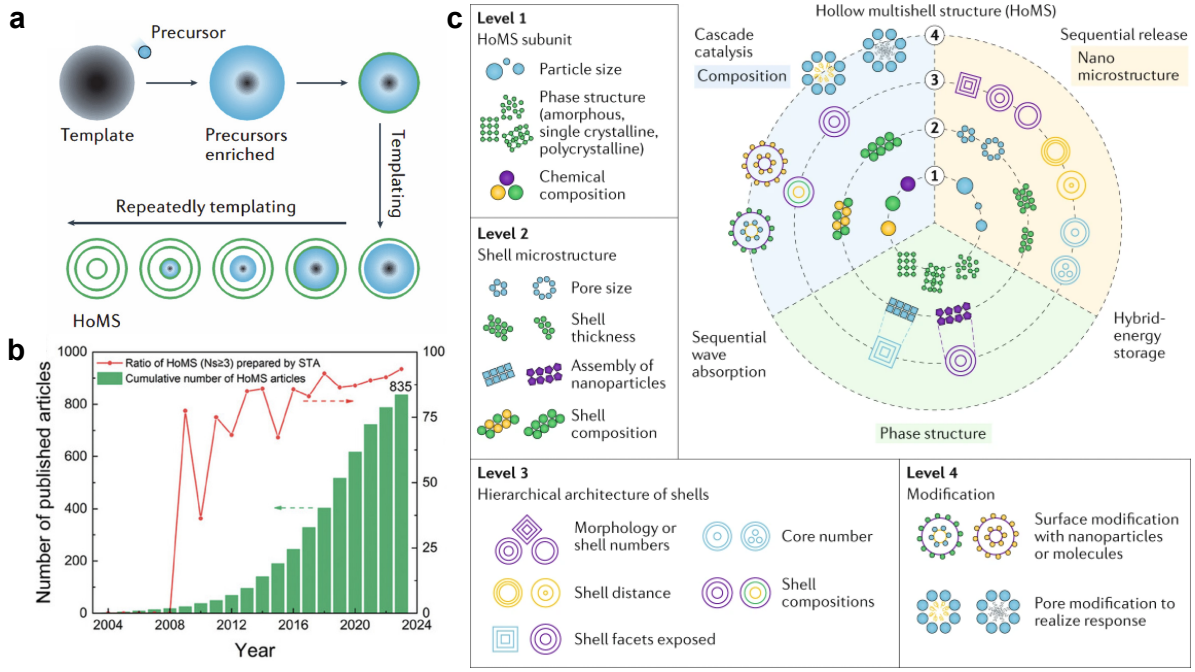

Figure 6 Schematic diagram of the controllable preparation, research development, and key design parameters of hollow multishelled structure (HoMS). (a) Schematic diagram of the sequential templating approach (STA). Reproduced with permission from Ref. [83]. Copyright©2022, Springer Nature. (b) Annual publication growth of HoMS-related research and the proportion change of those prepared using STA. Reproduced with permission from Ref. [84]. Copyright©2023, John Wiley and Sons. (c) Tunable parameter system of HoMS (subunits, single-shell microstructure, multishell hierarchical architecture, and post-modification) and its correlation with typical functions/applications. Reproduced with permission from Ref. [83]. Copyright©2022, Springer Nature.

deposition, passivation, and stress accumulation. In this context, HoMS are particularly attractive because their multishelled architecture can simultaneously regulate transport, reaction, and mechanical stability within a single framework. Specifically, interconnected multishell channels can homogenize ion flux and suppress tip-induced dendrite growth, internal cavities can accommodate deposition and buffer volume changes, and tunable shell structures can confine interphase evolution and inhibit the continuous thickening of passivation layers. Through this synergistic regulation, HoMS can effectively slow resistance buildup and prevent the evolution from reversible interfacial fluctuations to irreversible degradation.

Wei *et al*. [90] proposed a transferable HoMS composite membrane. Dense packing of HoMS can form continuous ion-conduction channels within the interfacial layer. This structure homogenizes ion distribution at the interface and reduces current hot spots induced by the tip effect. Meanwhile, the polymer matrix provides mechanical compliance and deformation space. It helps maintain conformal contact during plating/stripping and buffers stress accumulation. This reduces cracking, delamination, and local failure caused by volume changes. Therefore, HoMS materials function beyond a simple coating. They enable synergistic channel construction and mechanical buffering. Through this synergy, deposition can shift from disordered local stacking to more controllable and uniform growth, thereby suppressing the coupled evolution of dendrites and side reactions.

As illustrated in Figure 7a [90], it explains how a transferable HoMS composite membrane regulates Li deposition. The HoMS membrane provides accessible pore space and promotes the formation of a more stable SEI. It also enables selective transport with high ionic conductivity but low electronic conductivity.

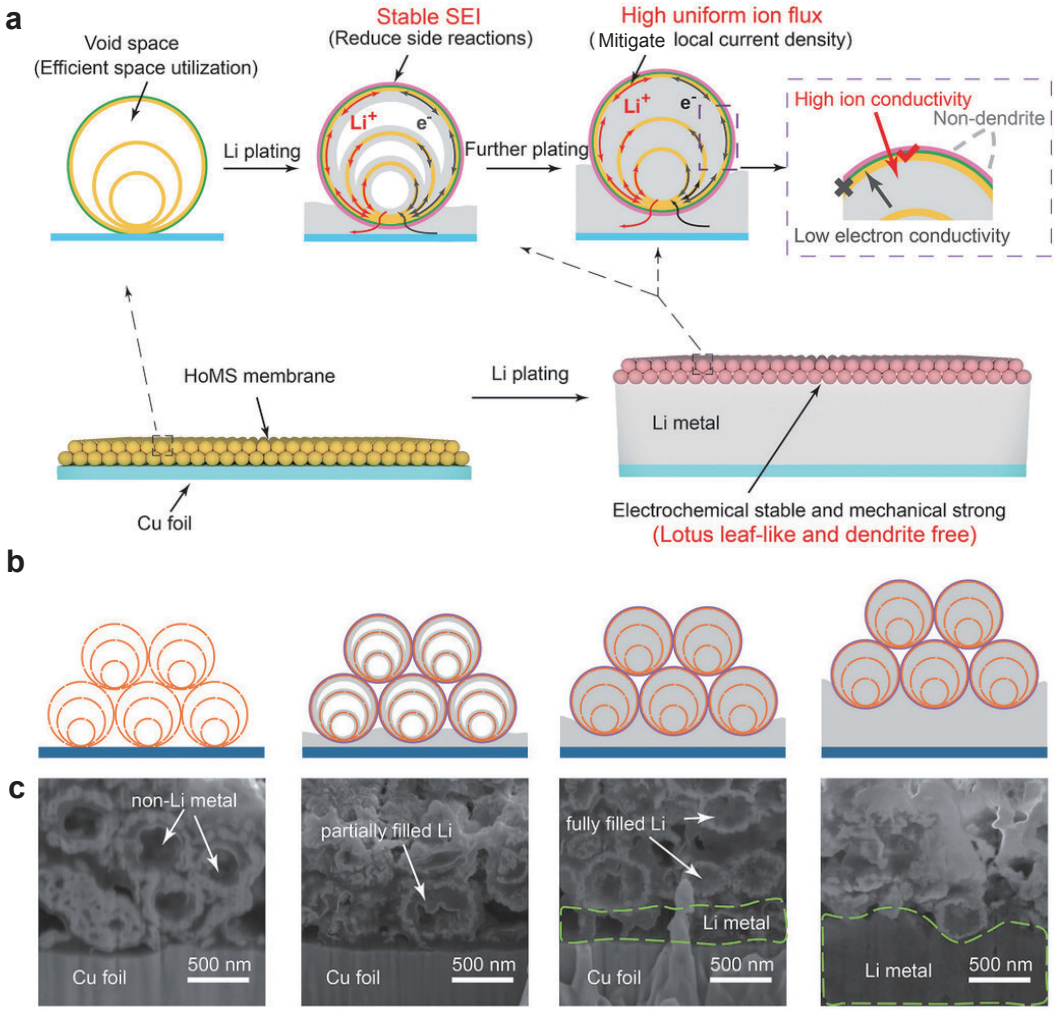

Figure 7 (a) Schematic diagram showing the advantages of a relocatable HoMS-based composite membrane for Li metal anode, which can simultaneously inhibit Li dendrites and stabilize the SEI; (b) schematic diagrams and (c) SEM images of 3S-Cu HoMS electrode with different amounts of deposited Li metal. Reproduced with permission from Ref. [90]. Copyright©2024, John Wiley and Sons.

This selectivity delivers a more uniform ion flux, lowers local current density, suppresses dendrite growth, and promotes dense and flat Li deposition at the membrane/current-collector interface (Figure 7a, b). The cross-sectional SEM images (Figure 7c) show the deposition evolution from "unfilled → partially filled → filled". Ultimately, a continuous lotus-leaf-like Li layer is formed with improved electrochemical and mechanical stability, enabling a dendrite-free and long-life Li metal anode. This strategy provides useful design inspiration for stabilizing metal anode interfaces in non-aqueous MABs (e.g., Li-air batteries). Its core principles (flux homogenization + buffering + controlled SEI localization) can also be extended to MAB systems by integrating corrosion-inhibiting chemistries on shell surfaces.

Zhao *et al*. [91] designed a "multicore@multishell" architecture to achieve more refined interfacial stabilization via functional division between inner and outer shells (Figure 8). A general synthesis strategy for multicore@multishell hollow composites shows that the inner shell can constrain the direction of volume change of active materials, while the outer shell preserves the integrity of the overall structure and interface,

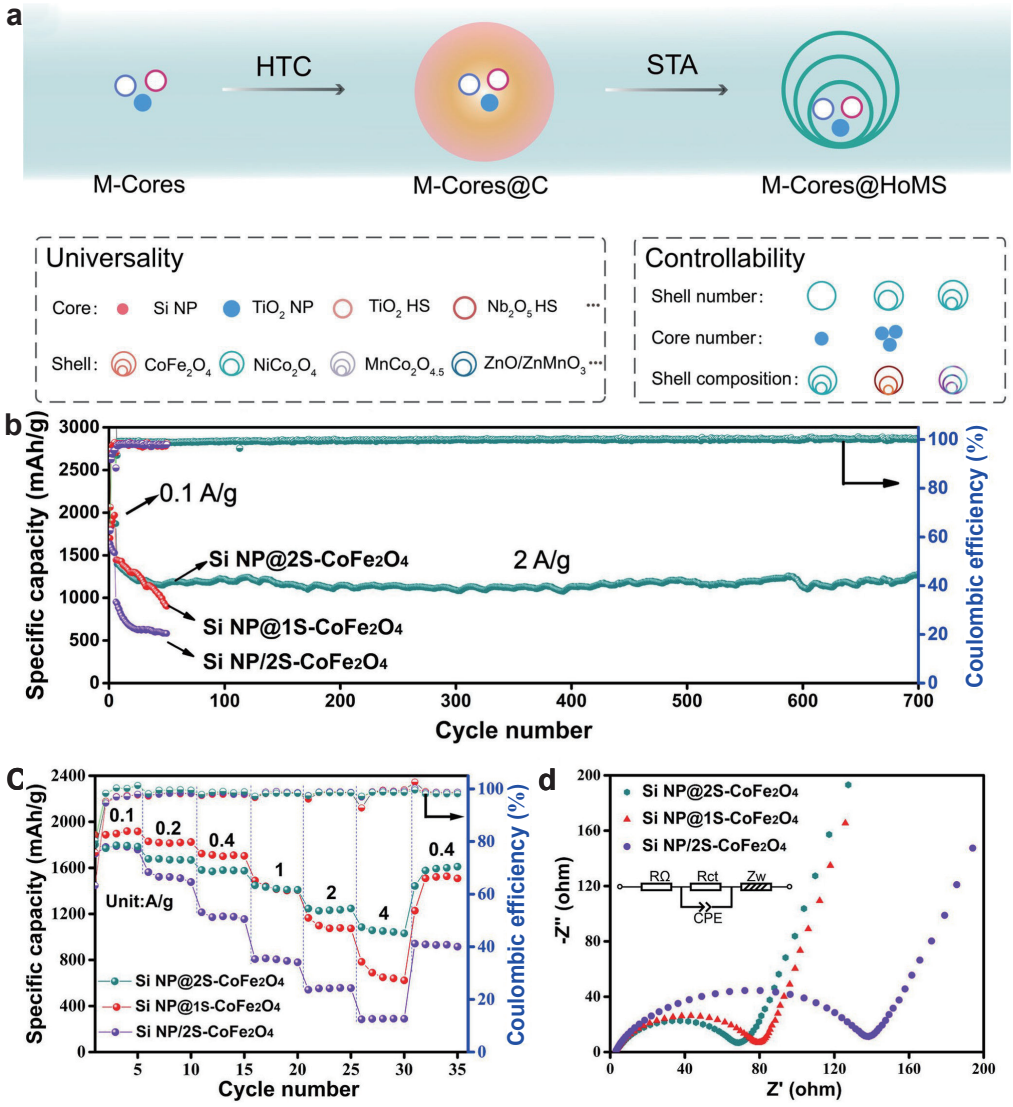

Figure 8 (a) Schematic illustration of the general preparation process of multiple cores@multiple shells composite (note: M-cores means multiple cores, HTC means hydrothermal carbonization). (b) The long-term cycling performance of Si NP@2S-$CoFe_2O_4$. (c) Rate capability performance. (d) EIS measurement before the 1st cycle with the equivalent circuit model inserted. Reproduced with permission from Ref. [91]. Copyright©2021, John Wiley and Sons.

thus improving cycling stability in lithium-ion batteries [91]. Figure 8a shows a universal and controllable construction route for multicore@HoMS (M-Cores@HoMS). A carbon layer is first formed on core particles by hydrothermal carbonization (HTC) (M-Cores@C). Subsequent treatment induces stepwise formation of multiple shells. Therefore, the shell number, core number, and shell composition can be tuned. Electrochemical results for Si-core@double-shell $CoFe_2O_4$ show high specific capacity and stable Coulombic efficiency during long cycling, as well as improved kinetics and lower interfacial charge-transfer resistance in rate tests and impedance spectra (Figure 8b–d) [91].

Based on this multicore@multishell concept, anode-side passivation in MABs can be understood as an uncontrolled accumulation of interfacial reaction products across spatial and temporal scales [92]. This

accumulation leads to continuous thickening of dense passivation films, hindered ion transport, and a rapid increase in interfacial resistance. By analogy to the tunable hierarchy of multishelled structures, a multi-layer interfacial architecture with functional division can be built on the anode surface. This approach can transform passivation from uncontrolled spontaneous growth to a predictable, regulated evolution. In this design, the outer shell serves as a chemical barrier to slow corrosion and side reactions and to suppress the rapid spreading of passivation products on the metal surface. Meanwhile, internal cavities buffer deposition and volume changes, which helps avoid repeated cracking/spallation and the vicious cycle of re-passivation triggered by stress concentration. As a result, the passivation layer is more likely to remain thin and uniform, and resistance growth is significantly slowed. In addition, cavities and inter-shell spaces can act as product reservoirs to reduce the risk of abrupt interfacial blockage. The multi-core concept further suggests introducing immobilized functional components within inner particles. Ion-philic components, corrosion inhibitors, or particles that regulate passivation products can be embedded in the multishell framework or inter-shell space. This disperses reaction hot spots and guides products to preferentially form on the outer shell surface or within inter-shell regions. It reduces the tendency to form a dense, dead film on the metal surface. With gradient shells and hierarchical pore design, the interfacial layer can tolerate deposition-induced blockage while maintaining ion transport. This yields a more stable, thinner, and more uniform passivation layer and effectively suppresses resistance accumulation and performance decay.

In summary, for anode passivation, the design of HoMS for metal-anode interfaces should focus on three main aspects: constructing parallel and interconnected ion-transport channels through multishelled architectures to homogenize ion flux, spatially dispersing passivation products within cavities to avoid the direct formation of dense films on the metal surface, and introducing compliant or reinforced structures to buffer stress and maintain interfacial integrity. Meanwhile, the shells should preserve electrolyte mass transport while suppressing electron leakage, thereby reducing side reactions, confining interphase evolution to more controllable regions, and slowing resistance accumulation. These principles provide a clear basis for the structural design and validation of HoMS-based interfacial candidates for stabilizing metal anodes in MABs.

HoMS provides a high surface area to enhance catalytic activity

For aqueous MABs, HoMS-based regulation of air-cathode interfaces should address the coupled challenges of precipitation-induced blockage, shrinkage of the triple-phase reaction zone, and the mismatch between interfacial kinetics and mass transport. In aqueous systems, a water/solid/gas triple-phase interface is formed at the air cathode, and its effective area and connectivity directly determine active-site accessibility as well as the transport efficiency of reactants and products [93–95]. During practical operation, accumulated discharge products can gradually block pores, disrupt oxygen/electrolyte transport pathways, and reduce the effective reaction zone, thereby increasing polarization and limiting reversibility. In this context, the multishell and cavity architecture of HoMS can provide internal space to accommodate precipitates and delay pore clogging, while preserving the continuity of triple-phase channels. Meanwhile, the coupled regulation of shell porosity, thickness, and pore-size gradient can balance oxygen diffusion and electrolyte wetting, avoid local flooding or dryness, and thus stabilize the reaction zone. Hierarchical channels can further enable functional division, in which larger pores favor oxygen diffusion and gas exchange, smaller pores help maintain electrolyte imbibition and ion migration, thereby sustaining transport continuity and weakening con-

centration polarization under high product loading. Beyond transport regulation, HoMS can also improve the catalytic microenvironment for aqueous ORR/OER. Their multishelled architectures provide high surface area, controllable surface exposure, and structurally defined platforms for introducing defects or heterostructures and coupling them with conductive networks. This facilitates the co-optimization of intermediate adsorption, interfacial charge transfer, and structural stability, thereby lowering air-cathode polarization and improving reversible reaction kinetics [96]. Although much of the current evidence is derived from cross-system studies, these results consistently show that HoMS-based hosts, catalysts, or interlayers can preserve transport channels and promote interfacial conversion even under severe product accumulation, supporting HoMS as a promising structural platform for aqueous air cathodes. In addition, surface-chemistry reconstruction strategies provide useful guidance for further fine regulation of catalytic interfaces [97]. Overall, the structural features of HoMS are well matched to the main air-cathode challenges in aqueous MABs, because they can simultaneously alleviate pore blockage, stabilize the triple-phase reaction zone, and mitigate the mismatch kinetic and transport through coupled regulation of transport pathways, product distribution, and catalytic microenvironment.

Jiao *et al*. [98] designed a metal-organic framework (MOF)-derived dodecahedral HoMS (Figure 9). In alkaline rechargeable systems, the triple-shelled Mn-Co oxide hollow dodecahedron can distribute mechanical stress across multiple shells and provide continuous mass-transport pathways. It therefore delivers markedly improved cycling stability and rate performance (Figure 9a). As shown in Figure 9b–g, owing to sufficient exposure of active sites, short electron/ion transport distances, and effective spatial buffering and structural stabilization, the material exhibits favorable kinetics and rate performance at different scan rates and current densities. It also maintains a relatively stable capacity output during long-term cycling.

Beyond the direct geometric advantages of HoMS, recent studies suggest that their greater value lies in serving as a structural platform for multi-strategy synergistic regulation. In such systems, HoMS do not merely function as hollow multishelled architectures for increasing surface area or buffering structural changes; rather, they can be integrated with defect engineering, heterointerface construction, coordination-environment regulation, and surface-coating design to co-optimize catalytic activity, mass/electron transport, and interfacial stability. In this context, the performance enhancement does not arise from a simple addition of individual strategies, but from functional coupling across multiple levels: HoMS provides accessible reaction space, continuous transport pathways, and structural robustness, while additional modification strategies tailor the local electronic structure, intermediate adsorption, and interfacial reactivity. Therefore, the design value of HoMS-based systems lies in enabling multilevel cooperation among structural confinement, transport regulation, and catalytic-site optimization, offering a more instructive route for interface engineering than any single strategy alone.

Liu *et al*. [99] reported the Fe-N_4SP/NPS-HC catalyst (Figure 10), in which regulation of the Fe coordination environment was combined with the design of a hollow carbon nanocage structure to improve ORR performance. In this system, the axial S atom in the first coordination shell and the adjacent P atom in the second coordination shell jointly tune the local electronic structure around the Fe-N_4 site, lower the d-band center of the Fe site, and enhance spin polarization. As a result, the adsorption and desorption of oxygen-containing intermediates, especially *OH, are optimized. At the same time, the hollow carbon nanocage structure is favorable for electrolyte penetration, reactant diffusion, and active-site exposure (Figure 10a). Benefiting from these features, the catalyst shows better ORR polarization behavior in 0.1 M

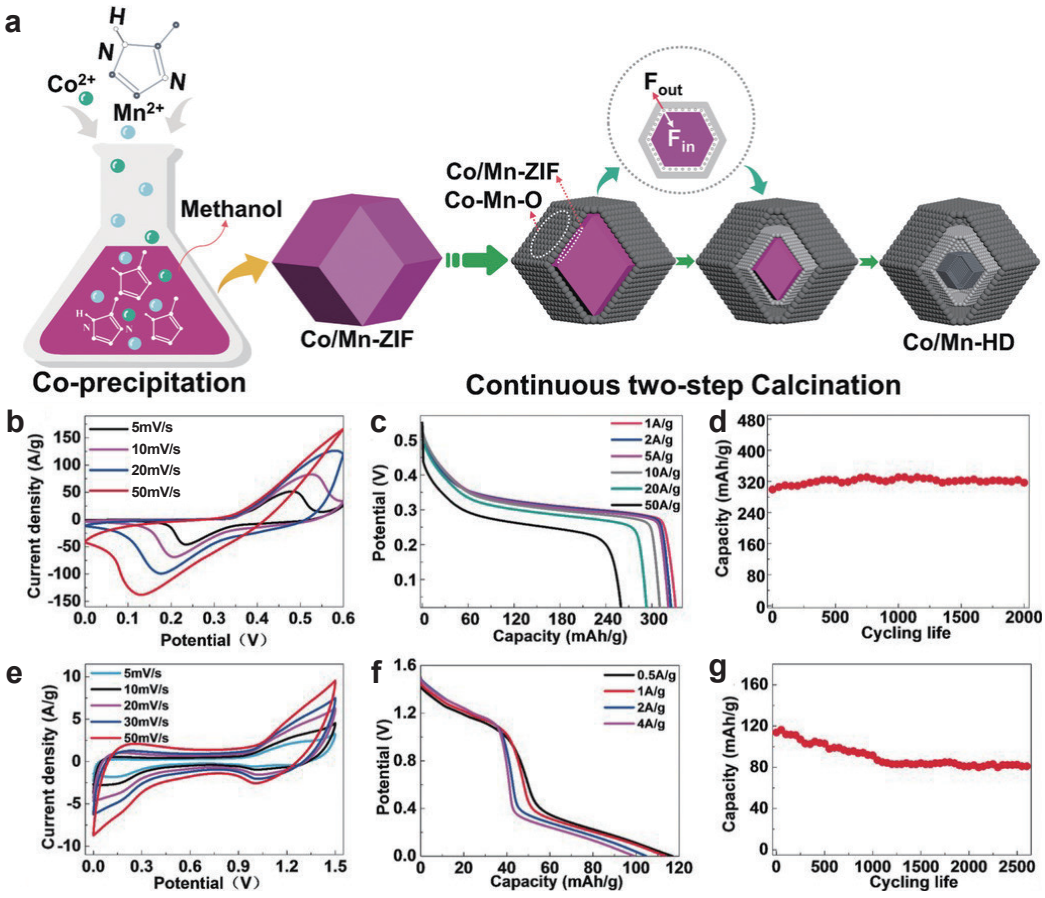

Figure 9 (a) The synthesis mechanism of triple-shelled Co/Mn-HD. The electrochemical performance of triple-shelled Co/Mn-HD as electrode material in a three-electrode system: (b) cyclic voltammetry curves; (c) galvanostatic charge-discharge curves; (d) cycling life. Co/Mn-HD as electrode material in an alkaline rechargeable battery: (e) cyclic voltammetry curves; (f) galvanostatic charge-discharge curves; (g) cycling stability. Reproduced with permission from Ref. [98]. Copyright©2018, John Wiley and Sons.

KOH, and its polarization curve is located in a higher potential region (Figure 10b). Its half-wave potential reaches 0.912 V, which is clearly higher than those of Fe-N_4P/NPC, Fe-N_4/NC, and Pt/C (Figure 10d). At the same time, it shows a small Tafel slope of 39.18 mV dec^{-1} (Figure 10c) and a kinetic current density of 60 mA cm^{-2} at 0.85 V (Figure 10d), indicating faster ORR kinetics. In addition, the catalyst has an electron transfer number close to 4 and an H_2O_2 yield below 6% (Figure 10e). It also shows a double-layer capacitance of 19.80 mF cm^{-2} (Figure 10f). After 10000 cycles, the half-wave potential decreases by only 17 mV (Figure 10g), indicating good stability. These results show that regulation of the coordination environment improves the intrinsic catalytic activity of the Fe active sites, while the hollow hierarchical structure further enhances interfacial mass transport and active-site utilization. The combination of these two effects leads to the improved ORR performance [99].

HoMS-based coatings enable selective transport and improve interfacial stability

For separator/electrolyte interfaces, HoMS can serve either as a functional coating layer or as a composite

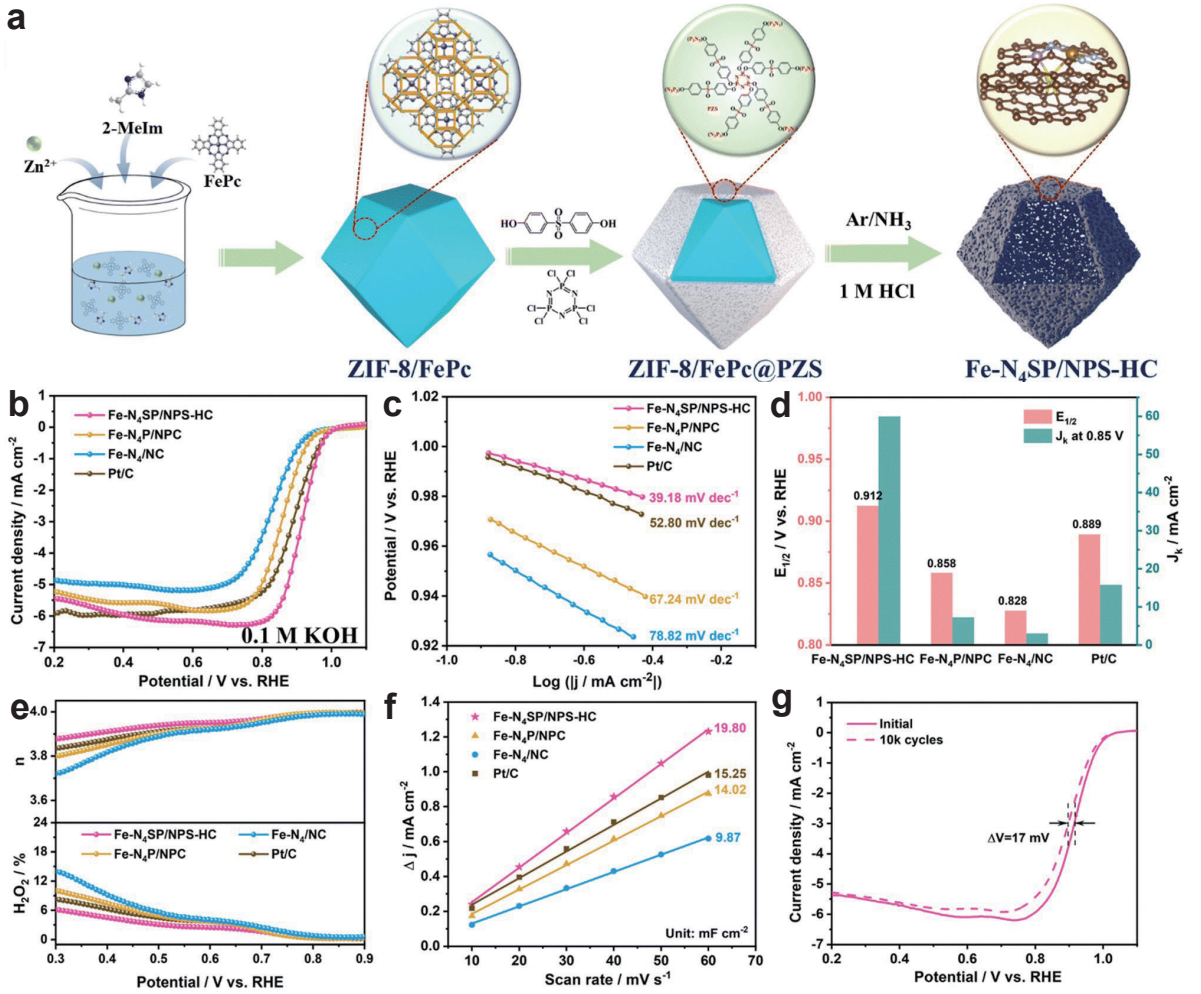

Figure 10 Synthesis route of Fe-N_4SP/NPS-HC single-atom catalyst and its ORR electrocatalytic performance. (a) Schematic diagram of catalyst synthesis; (b) comparison of ORR polarization curves in 0.1 mol L^{-1} KOH; (c) Tafel curves; (d) comparison of half-wave potential ($E_{1/2}$) and kinetic current density at 0.85 V; (e) hydrogen peroxide yield; (f) double-layer capacitance (C_{dl})/ECSA characterization; (g) cycling durability. Reproduced with permission from Ref. [99]. Copyright©2024, Royal Society of Chemistry.

filler to address the coupled challenges of pore blockage, ion-flux heterogeneity, species crossover, and mechanical instability. In practical MABs, deposits and dissolved species can progressively obstruct separator pores, increase transport resistance, and disturb local current distribution, thereby aggravating anode-side interfacial failure. In this context, HoMS design can be developed from multiple aspects, including anti-clogging and product buffering through multishell cavities, ion-flux homogenization through hierarchical transport channels, adsorption and interception of unfavorable species by tunable shell surfaces and functional sites, enhanced puncture resistance, and coordinated wetting with the electrolyte. Through these combined functions, HoMS can reduce resistance accumulation at the separator side, preserve ion-transport continuity, and suppress anode-interface instability induced by non-uniform flux.

Hierarchical hollow structures can serve as multifunctional building blocks for interfacial layers or functional separator coatings. For example, a TiN multilayer hollow structure used for separator modification provides multiple spatial barriers and abundant adsorption sites, while also constructing short and continuous

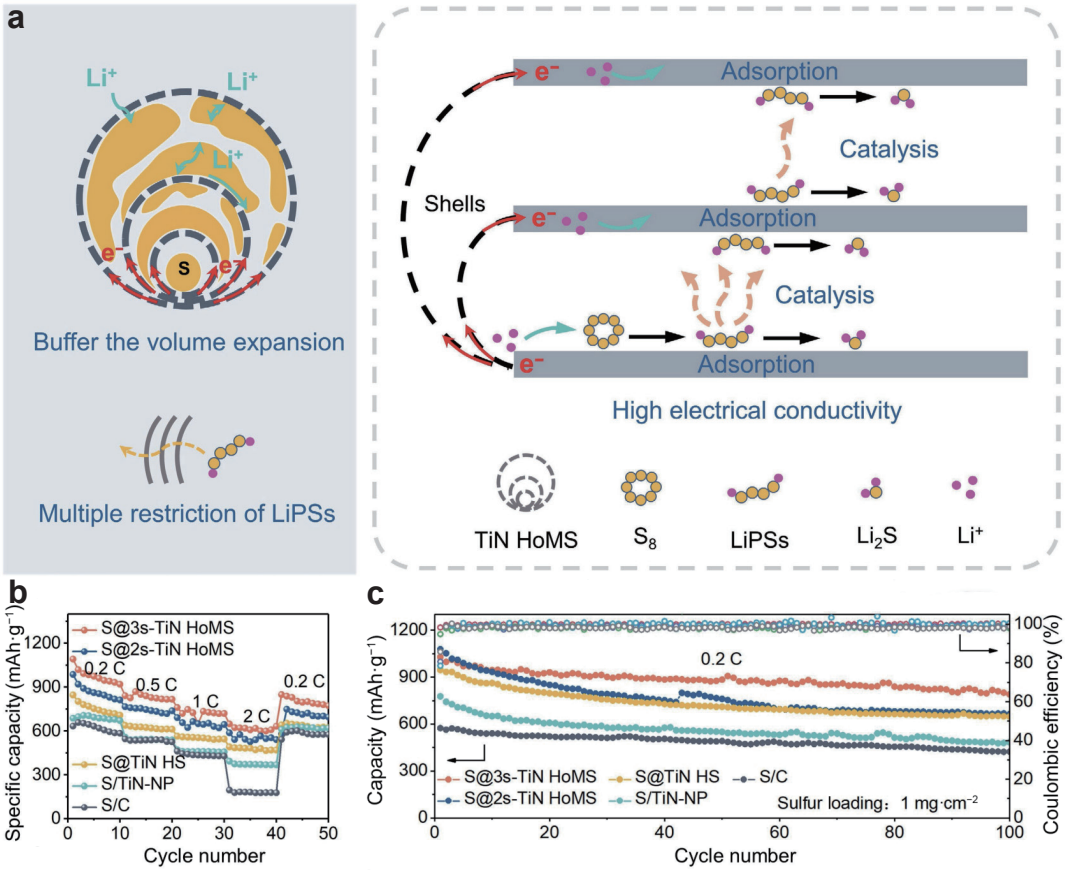

Figure 11 (a) Schematic illustration of the electrode process for the S@3S-TiN HoMS cathode; (b) rate capabilities of S@TiN HoMS, S@TiN HS, S/TiN-NP, and S/C electrodes tested at 0.2, 0.5, 1, and 2 C; (c) cycling performance of S@TiN HoMS, S@TiN HS, S/TiN-NP, and S/C at 0.2 C. Reproduced with permission from Ref. [100]. Copyright©2023, Springer Nature.

transport pathways. In addition, the high conductivity and surface catalytic activity of TiN can promote the rapid conversion of soluble polysulfides, thus markedly improving capacity retention and cycling stability [100]. As shown in Figure 11a, TiN HoMS plays two roles in Li-S batteries. On the one hand, its multiple shells and cavities buffer volume change during charge/discharge and provide multi-level confinement for soluble lithium polysulfides. On the other hand, supported by the conductive TiN network and its adsorption/catalytic sites, polysulfide conversion kinetics is accelerated, and the shuttle effect is weakened. Rate and cycling results show that S@TiN HoMS electrodes maintain high specific capacity and stable Coulombic efficiency at different rates, and they outperform control samples in long-term cycling (Figure 11b, c) [100]. Similarly, the introduction of N-doped carbon multilayer hollow structures into separator modification can, through the synergy of adsorption/confinement and hierarchical diffusion channels, suppress the migration of soluble species while maintaining fast ion transport, thereby balancing isolation and kinetic requirements [56]. Although this work mainly derives from separator/interface design in other energy-storage systems, its combined ideas of structural confinement, interfacial catalysis, and wetting regulation are also informative for metal-air batteries [101–103]. For example, a functional interlayer may regulate the local distribution of oxygen and electrolytes, reduce the sensitivity of mass transport to pore blockage, and suppress parasitic reactions at both electrodes, thereby improving overall operational stability.

Although this strategy was developed for Li-S batteries, its structure-function relationship provides useful inspiration for separator design in Zn-air batteries. In Zn-air systems, separator-side failure is also closely associated with species migration, deposit accumulation, transport interruption, and local flux heterogeneity. From this perspective, HoMS-based coatings may help regulate Zn-air separators in several ways: multi-shelled architectures can provide graded barriers and homogenize ion transport, internal cavities may buffer the accumulation of Zn-related deposits and delay pore blockage, and functional shell surfaces can be used to modulate the distribution of zincate species and other interfacial products. In addition, the hierarchical framework may enhance mechanical robustness and reduce separator-side instability during long-term cycling. Therefore, although the specific chemistry differs from that of Li-S systems, HoMS offers transferable structural design principles for constructing multifunctional separators in Zn-air batteries.

In addition to their roles in regulating cathode, anode, and separator interfaces, HoMS may also influence the local interfacial microenvironment, which is closely associated with ion distribution and reaction kinetics. Recent studies on electrolyte and interfacial regulation suggest a common principle that interfacial stability is closely related to the local distribution of ions and solvents, rather than being governed solely by bulk transport or structural features [104–106]. In particular, the organization of ion pairs or aggregates near the interface can affect desolvation behavior, interphase formation, and reaction uniformity, thereby determining interfacial kinetics and stability. Although these studies are mainly based on electrolyte design, they highlight the importance of regulating the local microenvironment at battery interfaces. From this perspective, HoMS may provide more than structural confinement and transport pathways. Their confined and hierarchical architectures could influence the local distribution of ions, solvents, and intermediates, thereby regulating ion flux, interfacial reactions, and interphase evolution. This provides a possible link between structural design and interfacial reaction kinetics in metal-air batteries.

In solid-state metal-air batteries, the key interfacial problems differ from those in liquid systems [51,52]. Besides dendrite growth and side reactions at the metal anode, poor solid-solid contact and high interfacial resistance at the metal/electrolyte and electrolyte/air-cathode interfaces strongly limit ion transport and reaction kinetics [74]. In this context, HoMS may provide useful design inspiration because its multishelled porous architecture can provide continuous ion-transport pathways, enlarge effective interfacial contact, and buffer stress accumulation during repeated deposition/stripping. In addition, when incorporated into composite solid electrolytes, HoMS fillers can increase active interaction sites, suppress polymer crystallinity, and improve both ionic conductivity and mechanical stability, as demonstrated by ZnO HoMS in PEO-based polymer electrolytes [107]. Therefore, although direct studies of HoMS in solid-state metal-air batteries remain limited, their structure-function relationship is highly relevant to the major bottlenecks at solid-state interfaces.

The design priorities and interfacial roles of HoMS also vary across non-aqueous, aqueous, and solid-state MAB systems. To provide a clearer cross-system comparison, a summary is presented in Table 1.

As shown in Table 1, HoMS offers several common advantages across different MAB systems, including transport regulation, product buffering, and interfacial stabilization. However, their dominant roles are system-dependent: in non-aqueous systems, they mainly suppress side reactions and regulate discharge-product deposition; in aqueous systems, they maintain transport continuity and stabilize multiphase interfaces, while in solid-state systems, they are more closely associated with improving solid-solid contact and mechanical stability.

Table 1 Comparison of HoMS-based interfacial regulation strategies in non-aqueous, aqueous, and solid-state metal-air batteries

MAB system	Main interfacial challenge	HoMS design priority	The main function of HoMS	Typical performance benefit
Non-aqueous MABs [74]	Parasitic reactions, unstable metal/electrolyte interface, uncontrolled discharge-product deposition, and pore blockage	Spatial confinement of discharge products, construction of continuous ion/electron pathways, stabilization of reactive metal interfaces	Regulating discharge-product distribution, suppressing side reactions, homogenizing ion flux, and stabilizing interphase evolution	Reduced polarization and side reactions, improved cycling reversibility, and interfacial stability
Aqueous MABs [108]	Precipitation-induced pore blockage, shrinkage of triple-phase reaction zone, corrosion/ passivation, and non-uniform ion flux	Buffering of precipitate accumulation, maintenance of gas-liquid-solid transport pathways, catalytic-site optimization, and ion-flux homogenization	Preserving transport continuity, stabilizing the reaction zone, promoting ORR/OER kinetics, and mitigating corrosion/ passivation-related degradation	Improved rate capability, reduced concentration polarization, enhanced cycling stability, and interface durability
Solid-state MABs [52]	Poor solid-solid contact, high interfacial resistance, mechanical degradation, and stress accumulation	Increasing interfacial contact area, introducing compliant buffer structures, and improving interface compatibility	Reducing contact resistance, buffering interfacial stress, and stabilizing solid-solid interfaces	Lower interfacial impedance, improved contact stability, and better structural durability

SUMMARY AND OUTLOOK

In summary, this review systematically compares the reaction processes and interfacial evolution characteristics of non-aqueous, aqueous, and solid-state MABs, clarifying the synergistic regulatory role of the metal anode side, the air cathode side, and internal contact regions in governing electron/ion transport, oxygen supply, and the formation and conversion of reaction intermediates, all of which directly determine the energy efficiency and cycle life of MABs. This review also highlights the recurrent interfacial failure pathways that are common across different MAB systems: (1) The accumulation of discharge products and by-products narrows or even blocks the pores of the air electrode, gradually reducing its usable reaction region; (2) electrolyte decomposition and side reactions continuously increase interfacial resistance, undermining charge transfer efficiency; (3) on the metal anode, corrosion or passivation layer growth often occurs alongside non-uniform deposition, dendrites formation, and the generation of "dead metal", which degrade anode performance; (4) volume changes and stress buildup during cycling lead to interfacial delamination, cracking, and poor contact, further accelerating polarization and capacity fading. Based on these observations, this review summarizes the common modification strategies for the air electrode, metal anode, and separator/electrolyte interface, while clarifying their practical application boundaries. It also points out the remaining key challenges, including insufficient quantitative understanding of interfacial mechanisms, limited compatibility among different modification strategies, and inadequate performance validation under engineering-relevant practical conditions. Additionally, this review emphasizes the HoMS as a potential materials platform, whose multi-level cavities can provide buffering space for reaction products to slow down pore blockage, multishell pathways can support more continuous mass transport, and structural buffering capacity may reduce the risks of cracking and delamination, offering a tunable route to stabilize multiphase interfaces in MABs.

Looking ahead, the practical value of HoMS in MABs will depend on moving from experience-based design to a clearer, more predictable design strategy. Compared with simple surface modification methods,

HoMS possesses more adjustable structural features, including shell number, shell thickness, cavity spacing, pore structure, particle size, and the distribution of defects or heterointerfaces. These structural features not only alter the material morphology but also significantly regulate interfacial functions: for instance, shell thickness and pore structure can directly influence oxygen diffusion and electrolyte wetting at the air cathode; shell number and cavity spacing can affect the storage of reaction products, ion migration behavior, and growth of passivation layers on the anode; charge transfer efficiency, and local stress release. Thanks to these unique advantages, HoMS can simultaneously regulate product accumulation, maintain unobstructed transport pathways, and improve both chemical and mechanical stability within a single material system, addressing multiple interfacial challenges in MABs.

In the future, artificial intelligence (AI) technologies are expected to establish robust links between the structural features of HoMS, interface characterization results, battery performance, and operating conditions, thereby facilitating the efficient screening and design of superior materials to address key issues such as product blockage, corrosion, passivation, and uneven reactions. It is also crucial to incorporate not only successful modification cases, but also failed or ineffective ones into research summaries, as these cases can deepen the understanding of the intrinsic mechanisms underlying interfacial instability. Building such comprehensive databases will improve the accuracy and usefulness of AI-guided material design, accelerate the optimization of HoMS-based interfacial materials, and promote their practical application in MABs, ultimately advancing the development of high-performance, environmentally benign MAB systems for carbon-neutral energy storage.

Funding

This work was supported by the National Key Research and Development Program of China (2022YFA1204500 and 2022YFA1204502), the National Natural Science Foundation of China (22293043, 92572205, 52272097, 52301296, W2512061 and 52261160573), the Shenzhen University 2035 Program for Excellent Research (2024B005), the Beijing Natural Science Foundation (Z230019 and 2242019) and the IPE Project for Frontier Basic Research, China (QYJC-2023-08). D.W. thanks the financial support from the Outstanding Scientific and Technological Innovation Talents Training Fund in Shenzhen.

Author contributions

P.S. completed the main writing of the manuscript. D.L. was responsible for collecting and integrating the relevant references. D.H. and J.W. provided revision suggestions for the initial draft. J.W., D.W. and R.Y. designed the manuscript outline, offered professional guidance, and revised the initial draft.

Conflict of interest

The authors declare no conflict of interest.

References

1 Park J, Son Y. Recent progress of materials design and engineering of aqueous metal-air batteries. *Korean J Chem Eng* 2025; **42**: 1491–1505.

2 Rahman MA, Wang X, Wen C. High energy density metal-air batteries: A review. *J Electrochem Soc* 2013; **160**: A1759–A1771.

3 McKerracher RD, Ponce de Leon C, Wills RGA, *et al.* A review of the iron–air secondary battery for energy storage.

ChemPlusChem 2014; **80**: 323–335.

4 Dhanabalan K, Sriram G, Oh TH. An overview of electrocatalysts derived from recycled lithium-ion batteries for metal–air batteries: A review. *Energies* 2025; **18**: 4933.

5 Ma B, Hong D, Wei X, *et al.* Breaking the polarization bottleneck: Innovative pathways to high-performance metal–air batteries. *Batteries* 2025; **11**: 315.

6 Liu J, Ma B, Chen Z, *et al.* Novel strategies for low overpotential metal–air batteries. *Chem Commun* 2025; **61**: 14340–14353.

7 Wang W, Yu T, Cheng Y, *et al.* Field-assisted metal-air batteries: Recent progress, mechanisms, and challenges. *Nano Energy* 2024; **125**: 109550.

8 Chi X, Li M, Di J, *et al.* A highly stable and flexible zeolite electrolyte solid-state Li–air battery. *Nature* 2021; **592**: 551–557.

9 Chen R, Li Q, Yu X, *et al.* Approaching practically accessible solid-state batteries: Stability issues related to solid electrolytes and interfaces. *Chem Rev* 2020; **120**: 6820–6877.

10 Barman M, Pal M, Biswas R, *et al.* A comprehensive review of metal-air batteries: Mechanistic aspects, advantages and challenges. *Catal Today* 2025; **451**: 115229.

11 Li Y, Lu J. Metal–air batteries: Will they be the future electrochemical energy storage device of choice? *ACS Energy Lett* 2017; **2**: 1370–1377.

12 Nsanzimana JMV, Cai L, Jiang Z, *et al.* Engineering bifunctional catalytic microenvironments for durable and high-energy-density metal–air batteries. *Nano-Micro Lett* 2025; **17**: 294.

13 Wang Y, Li S, Li M, *et al.* Advances of the bifunctional electrocatalyst toward oxygen reduction/evolution reaction. *J Energy Chem* 2026; **114**: 574–607.

14 Qahtan TF, Alade IO, Rahaman MS, *et al.* Trends in metal-air battery research: Clusters, and future directions. *J Alloys Compd* 2025; **1022**: 179617.

15 Lyu L, Fan W, Shen J, *et al.* Bridging anode and cathode interfaces: Integrated interfacial strategies for aqueous metal–air batteries. *ACS Energy Lett* 2026; **11**: 1538–1570.

16 Minj NC, Mittal S, Yadav S, *et al.* High-entropy alloy-catalyzed bifunctional electrocatalysis of H_2 and O_2 involving reactions. *Chem Mater* 2026; doi: 10.1021/acs.chemmater.5c02763.

17 Ma N, Xiong Y, Wang Y, *et al.* A review of advancements in theoretical simulation of oxygen reduction reaction and oxygen evolution reaction single-atom catalysts. *Mater Today Sustain* 2024; **27**: 100876.

18 Yao M, Li N, Wang M, *et al.* 11-Electron transfer vanadium diboride employed as an anode of air batteries: Status, progress, and challenges. *New J Chem* 2025; **49**: 4286–4297.

19 Worku AK, Alemu MA, Ayele DW, *et al.* Recent advances in MXene-based materials for high-performance metal-air batteries. *Green Chem Lett Rev* 2024; **17**: 2325983.

20 Yi S, Song X, Shen Y, *et al.* Research progress in alloy catalysts for oxygen reduction reaction. *J Alloys Compd* 2024; **1002**: 175258.

21 Zhao Z, Liu Y, Yu J, *et al.* Critical metrics for practical application-oriented rechargeable zinc-air batteries. *Curr Opin Electrochem* 2026; **55**: 101784.

22 Jiang L, Luo X, Wang D. A review on system and materials for aqueous flexible metal–air batteries. *Carbon Energy* 2023; **5**: e284.

23 Li J, Zhang K, Wang B, *et al.* Light-assisted metal–air batteries: Progress, challenges, and perspectives. *Angew Chem Int Ed* 2022; **61**: e202213026.

24 Li M, Bi X, Wang R, *et al.* Relating catalysis between fuel cell and metal-air batteries. *Matter* 2020; **2**: 32–49.

25 Su F, Wang Z, Wan J, *et al.* Recent advances in optoelectronic synapses: From advanced materials to neuromorphic applications. *Rare Met* 2025; **44**: 6807–6838.

26 Lu L, Li Q, Sun Y, *et al.* Research progress on biomass carbon as the cathode of a metal-air battery. *New Carbon Mater* 2023; **38**: 1018–1034.

27 Li H, Chen J, Fang J. Recent advances in wearable aqueous metal-air batteries: From configuration design to materials fabrication. *Adv Mater Technologies* 2023; **8**: 2201762.

28 Lu YT, Neale AR, Hu CC, *et al.* Divalent nonaqueous metal-air batteries. *Front Energy Res* 2021; **8**: 602918.

29 Xu Y, Xue H, Li X, *et al.* Application of metal-organic frameworks, covalent organic frameworks and their derivates for the metal-air batteries. *Nano Res Energy* 2023; **2**: e9120052.

30 Wen X, Zhang Q, Guan J. Applications of metal–organic framework-derived materials in fuel cells and metal-air batteries. *Coord Chem Rev* 2020; **409**: 213214.

31 Qiu Y, Li G, Zhou H, *et al.* Highly stable garnet $Fe_2Mo_3O_{12}$ cathode boosts the lithium–air battery performance featuring a polyhedral framework and cationic vacancy concentrated surface. *Adv Sci* 2023; **10**: 2300482.

32 Deng M, Höche D, Lamaka SV, *et al.* Mg-Ca binary alloys as anodes for primary Mg-air batteries. *J Power Sources* 2018; **396**: 109–118.

33 Timofeeva EV, Segre CU, Pour GS, *et al.* Aqueous air cathodes and catalysts for metal–air batteries. *Curr Opin Electrochem* 2023; **38**: 101246.

34 Liu J, Zhou M, Jin K, *et al.* Beyond metal–air battery, emerging aqueous metal–hydrogen peroxide batteries with improved performance. *Battery Energy* 2024; **3**: 20230049.

35 Zhang YL, Goh K, Zhao L, *et al.* Advanced non-noble materials in bifunctional catalysts for ORR and OER toward aqueous metal–air batteries. *Nanoscale* 2020; **12**: 21534–21559.

36 Yu J, Li BQ, Zhao CX, *et al.* Seawater electrolyte-based metal–air batteries: From strategies to applications. *Energy Environ Sci* 2020; **13**: 3253–3268.

37 Javed N, Noor T, Iqbal N, *et al.* A review on development of metal–organic framework-derived bifunctional electrocatalysts for oxygen electrodes in metal–air batteries. *RSC Adv* 2023; **13**: 1137–1161.

38 Liu Q, Pan Z, Wang E, *et al.* Aqueous metal-air batteries: Fundamentals and applications. *Energy Storage Mater* 2020; **27**: 478–505.

39 Liu A, Liang X, Ren X, *et al.* Recent progress in MXene-based materials for metal-sulfur and metal-air batteries: Potential high-performance electrodes. *Electrochem Energy Rev* 2022; **5**: 112–144.

40 Xia Q, Zhai Y, Zhao L, *et al.* Carbon-supported single-atom catalysts for advanced rechargeable metal-air batteries. *Energy Mater* 2022; **2**: 200015.

41 Wang H, Wei P, Wang J, *et al.* Hollow multishelled structure reviving lithium metal anode for high-energy-density batteries. *Chem Res Chin Univ* 2024; **40**: 428–436.

42 Mao D, Wang C, Li W, *et al.* Hollow multishelled structure: Synthesis chemistry and application. *Chem Res Chin Univ* 2024; **40**: 346–393.

43 Rao F, Xiao Q, Wei Y, *et al.* Balanced polysulfide containment and lithium ion transport in lithium-sulfur batteries via nitrogen-doped carbon hollow multi-shelled structures on modified separators. *Chem Res Chin Univ* 2024; **40**: 690–698.

44 Su F, Wan J, Wang D. Hollow multi-shelled structure photoelectric materials: multiple shells bring novel properties. *Chem Res Chin Univ* 2024; **40**: 413–427.

45 Hou P, Yang N, Wang D. Multi-functional hollow structures for intelligent drug delivery. *Chem Res Chin Univ* 2024; **40**: 394–412.

46 Wang H, Gong G, Sun G, *et al.* Regulating oxygen vacancy defects in heterogeneous NiO-$CeO_{2-\delta}$ hollow multi-shelled structure for boosting oxygen evolution reaction. *Chem Res Chin Univ* 2024; **40**: 475–483.

47 Wang J, Tang H, Wang H, *et al.* Multi-shelled hollow micro-/nanostructures: Promising platforms for lithium-ion batteries. *Mater Chem Front* 2017; **1**: 414–430.

48 Dilshad KAJ, Rabinal MK. Review on molecularly controlled design of electrodes for metal–air batteries: fundamental concepts and future directions. *Energy Fuels* 2023; **37**: 5689–5711.

49 Zhang C, Huang K. A comprehensive review on the development of solid-state metal–air batteries operated on oxide-ion chemistry. *Adv Energy Mater* 2021; **11**: 2000630.

50 Girishkumar G, McCloskey B, Luntz AC, *et al.* Lithium–air battery: Promise and challenges. *J Phys Chem Lett* 2010; **1**: 2193–2203.

51 Liu N, Liang Z, Yang F, *et al.* Flexible solid-state metal–air batteries: The booming of portable energy supplies. *ChemSusChem* 2023; **16**: e202202192.

52 Sun Q, Dai L, Luo T, *et al.* Recent advances in solid-state metal–air batteries. *Carbon Energy* 2023; **5**: e276.

53 Ogasawara T, Débart A, Holzapfel M, *et al.* Rechargeable Li_2O_2 electrode for lithium batteries. *J Am Chem Soc* 2006; **128**: 1390–1393.

54 Freunberger SA, Chen Y, Peng Z, *et al.* Reactions in the rechargeable lithium–O_2 battery with alkyl carbonate electrolytes. *J Am Chem Soc* 2011; **133**: 8040–8047.

55 Peng Z, Freunberger SA, Chen Y, *et al.* A reversible and higher-rate Li-O_2 battery. *Science* 2012; **337**: 563–566.

56 Lv X, Wang Z, Lai Z, *et al.* Rechargeable zinc–air batteries: Advances, challenges, and prospects. *Small* 2024; **20**: 2306396.

57 Salado M, Lizundia E. Advances, challenges, and environmental impacts in metal–air battery electrolytes. *Mater Today Energy* 2022; **28**: 101064.

58 Zhang Q, Wang C, Xie Z, *et al.* Defective/doped graphene-based materials as cathodes for metal–air batteries. *Energy Environ Mater* 2022; **5**: 1103–1116.

59 Aslam M, Noor T, Iqbal N. Advances in MXenes synthesis and MXenes derived electrocatalysts for oxygen electrode in metal-air batteries: A review. *Mater Sci Eng-B* 2023; **292**: 116400.

60 Milikić J, Nastasić A, Martins M, *et al.* Air cathodes and bifunctional oxygen electrocatalysts for aqueous metal–air batteries. *Batteries* 2023; **9**: 394.

61 Chen Y, Xu J, He P, *et al.* Metal-air batteries: Progress and perspective. *Sci Bull* 2022; **67**: 2449–2486.

62 Wang T, Yang T, Luo D, *et al.* High-energy-density solid-state metal–air batteries: Progress, challenges, and perspectives. *Small* 2024; **20**: 2309306.

63 Xu J, Ma Y, Xuan C, *et al.* Three-dimensional electrodes for oxygen electrocatalysis. *ChemElectroChem* 2022; **9**: e202101522.

64 Zhang S, Chen M, Zhao X, *et al.* Advanced noncarbon materials as catalyst supports and non-noble electrocatalysts for fuel cells and metal–air batteries. *Electrochem Energ Rev* 2021; **4**: 336–381.

65 Yang C, Ma X, Zhou J, *et al.* Recent advances in metal-organic frameworks-derived carbon-based electrocatalysts for the oxygen reduction reaction. *Int J Hydrogen Energy* 2022; **47**: 21634–21661.

66 Kwak WJ, Rosy WJ, Sharon D, *et al.* Lithium–oxygen batteries and related systems: Potential, status, and future. *Chem Rev* 2020; **120**: 6626–6683.

67 Alemu MA, Getie MZ, Worku AK. Advancement of electrically rechargeable multivalent metal-air batteries for future mobility. *Ionics* 2023; **29**: 3421–3435.

68 Li P, Wang H. Recent advances in carbon-supported iron group electrocatalysts for the oxygen reduction reaction. *New Carbon Mater* 2021; **36**: 665–682.

69 Li L, Zhu Q, Han M, *et al.* MOF-derived single-atom catalysts for oxygen electrocatalysis in metal–air batteries. *Nanoscale* 2023; **15**: 13487–13497.

70 Leong KW, Wang Y, Ni M, *et al.* Rechargeable Zn-air batteries: Recent trends and future perspectives. *Renew Sustain Energy Rev* 2022; **154**: 111771.

71 Tong F, Wei S, Chen X, *et al.* Magnesium alloys as anodes for neutral aqueous magnesium-air batteries. *J Magnesium Alloys* 2021; **9**: 1861–1883.

72 Liu Y, Sun Q, Li W, *et al.* A comprehensive review on recent progress in aluminum–air batteries. *Green Energy Environ* 2017; **2**: 246–277.

73 Yaqoob L, Noor T, Iqbal N. An overview of metal-air batteries, current progress, and future perspectives. *J Energy Storage* 2022; **56**: 106075.

74 Gu Z, Xin X, Men M, *et al.* Advancements, challenges, and prospects in rechargeable solid-state lithium-air batteries.

Batteries Supercaps 2023; **6**: e202300267.

75 Xie W, Zhu K, Yang H, *et al.* Advancements in achieving high reversibility of zinc anode for alkaline zinc-based batteries. *Adv Mater* 2024; **36**: 2306154.

76 Abarro JME, Gavan JNL, Loresca DED, *et al.* A tale of nickel-iron batteries: Its resurgence in the age of modern batteries. *Batteries* 2023; **9**: 383.

77 Zhang Y, Zheng X, Wang N, *et al.* Anode optimization strategies for aqueous zinc-ion batteries. *Chem Sci* 2022; **13**: 14246–14263.

78 Mainar A, Leonet O, Bengoechea M, *et al.* Alkaline aqueous electrolytes for secondary zinc-air batteries: An overview. *Int J Energy Res* 2016; **40**: 1032–1049.

79 Wang MY, Huang RB, Xiong JF, *et al.* Critical role and recent development of separator in zinc-air batteries. *Acta Physico-Chim Sin* 2024; **40**: 2307017.

80 Hu Z, Li G, Wang A, *et al.* Recent progress of electrolyte design for lithium metal batteries. *Batteries & Supercaps* 2020; **3**: 331–335.

81 Zhang J, Wan J, Wang J, *et al.* Hollow multi-shelled structure with metal–organic-framework-derived coatings for enhanced lithium storage. *Angew Chem Int Ed* 2019; **58**: 5266–5271.

82 Mao D, Wan J, Wang J, *et al.* Sequential templating approach: A groundbreaking strategy to create hollow multishelled structures. *Adv Mater* 2019; **31**: 1802874.

83 Wang J, Wan J, Yang N, *et al.* Hollow multishell structures exercise temporal–spatial ordering and dynamic smart behaviour. *Nat Rev Chem* 2020; **4**: 159–168.

84 Wei Y, Zhao D, Wang D. Mesoscience in hollow multi-shelled structures. *Adv Sci* 2024; **11**: e2305408.

85 Dong Z, Lai X, Halpert JE, *et al.* Accurate control of multishelled zno hollow microspheres for dye-sensitized solar cells with high efficiency. *Adv Mater* 2012; **24**: 1046–1049.

86 Wang J, Yang N, Tang H, *et al.* Accurate control of multishelled Co_3O_4 hollow microspheres as high-performance anode materials in lithium-ion batteries. *Angew Chem Int Ed* 2013; **52**: 6417–6420.

87 Qi J, Zhao K, Li G, *et al.* Multi-shelled CeO_2 hollow microspheres as superior photocatalysts for water oxidation. *Nanoscale* 2014; **6**: 4072–4077.

88 Wang J, Tang H, Ren H, *et al.* pH-regulated synthesis of multi-shelled manganese oxide hollow microspheres as supercapacitor electrodes using carbonaceous microspheres as templates. *Adv Sci* 2014; **1**: 1400011.

89 Chen M, Wang J, Tang H, *et al.* Synthesis of multi-shelled MnO_2 hollow microspheres via an anion-adsorption process of hydrothermal intensification. *Inorg Chem Front* 2016; **3**: 1065–1070.

90 Wei P, Wang H, Yang M, *et al.* Relocatable hollow multishelled structure-based membrane enables dendrite-free lithium deposition for ultrastable lithium metal batteries. *Adv Energy Mater* 2024; **14**: 2400108.

91 Zhao J, Wang J, Bi R, *et al.* General synthesis of multiple-cores@multiple-shells hollow composites and their application to lithium-ion batteries. *Angew Chem Int Ed* 2021; **60**: 25719–25722.

92 Xiao D, Lv X, Fan J, *et al.* Zn-based batteries for energy storage. *Energy Mater* 2023; **3**: 300007.

93 Shi F, Zhu X, Yang W. Micro-nanostructural designs of bifunctional electrocatalysts for metal-air batteries. *Chin J Catal* 2020; **41**: 390–403.

94 Li T, Peng X, Cui P, *et al.* Recent progress and future perspectives of flexible metal–air batteries. *SmartMat* 2021; **2**: 519–553.

95 Wang Y, Chu F, Zeng J, *et al.* Single atom catalysts for fuel cells and rechargeable batteries: Principles, advances, and opportunities. *ACS Nano* 2021; **15**: 210–239.

96 Yu Y, Liu Y, Peng X, *et al.* A multi-shelled CeO_2/Co@N-doped hollow carbon microsphere as a trifunctional electrocatalyst for a rechargeable zinc–air battery and overall water splitting. *Sustain Energy Fuels* 2020; **4**: 5156–5164.

97 Zhang Q, Cui C, Chen H, *et al.* Surface cobaltization for boosted kinetics and excellent stability of nickel-rich layered cathodes. *Natl Sci Open* 2024; **3**: 20240010.

98 Jiao C, Wang Z, Zhao X, *et al.* Triple-shelled manganese-cobalt oxide hollow dodecahedra with highly enhanced performance for rechargeable alkaline batteries. *Angew Chem Int Ed* 2019; **58**: 996–1001.

99 Liu J, Chen W, Yuan S, *et al.* High-coordination Fe–N_4 SP single-atom catalysts via the multi-shell synergistic effect for the enhanced oxygen reduction reaction of rechargeable Zn–air battery cathodes. *Energy Environ Sci* 2024; **17**: 249–259.

100 Xu W, Bi R, Yang M, *et al.* Hollow multishelled structural TiN as multi-functional catalytic host for high-performance lithium-sulfur batteries. *Nano Res* 2023; **16**: 12745–12752.

101 Zhao Y, Wang Y, Li J, *et al.* Thermodynamic and kinetic insights for manipulating aqueous Zn battery chemistry: Towards future grid-scale renewable energy storage systems. *eScience* 2025; **5**: 100331.

102 Wang Z, Chen J, Yang Z, *et al.* Zinc utilization rate in aqueous batteries: Regulation of interfacial thermodynamics and kinetics. *Natl Sci Open* 2025; **4**: 20250044.

103 Kang Z, Zhang Y. Materials science empowers carbon neutrality. *Natl Sci Open* 2024; **3**: 20240057.

104 Zhu Q, Yu D, Chen J, *et al.* A 110 Wh kg^{-1} Ah-level anode-free sodium battery at −40 °C. *Joule* 2024; **8**: 482–495.

105 Li Y, Wang J, Wang Y, *et al.* Sole-solvent high-entropy electrolyte realizes wide-temperature and high-voltage practical anode-free sodium pouch cells. *Adv Mater* 2025; **37**: e2419764.

106 Zhu Q, Wang J, Wu L, *et al.* A >200 Wh kg^{-1} anode-free Na pouch battery at −40°C enabled by manipulating electrolyte equilibrium. *Natl Sci Rev* 2025; **12**: nwaf124.

107 Ma Y, Bi R, Yang M, *et al.* Hollow multishelled structural ZnO fillers enhance the ionic conductivity of polymer electrolyte for lithium batteries. *J Nanopart Res* 2023; **25**: 14.

108 Rai S, Prachi P, Kant CR, *et al.* Metal-air batteries: From fundamental mechanisms to practical applications. *J Alloys Compd* 2025; **1033**: 180805.